Searching for the sources of excess extragalactic dispersion of FRBs

SUNIL SIMHA [0], ¹ KHEE-GAN LEE [0], ² J. XAVIER PROCHASKA [0], ^{1,2,3} ILYA S. KHRYKIN [0], ² YUXIN HUANG [0], ² NICOLAS TEJOS [0], ⁴ LACHLAN MARNOCH [0], ^{5,6,7,8} METIN ATA [0], ⁹ LUCAS BERNALES [0], ⁴ SHIVANI BHANDARI [0], ^{10,11}, *

JEFF COOKE [0], ^{12,8,6} ADAM T.DELLER [0], ¹² STUART D. RYDER [0], ^{5,7} AND JIELAI ZHANG [0], ^{12,13}

¹ University of California - Santa Cruz 1156 High St. Santa Cruz, CA, USA 95064
 ² Kavli IPMU (WPI), UTIAS, The University of Tokyo, Kashiwa, Chiba 277-8583, Japan
 ³ Division of Science, National Astronomical Observatory of Japan, 2-21-1 Osawa, Mitaka, Tokyo 181-8588, Japan
 ⁴ Instituto de Física, Pontificia Universidad Católica de Valparaíso, Casilla 4059, Valparaíso, Chile
 ⁵ School of Mathematical and Physical Sciences, Macquarie University, NSW 2109, Australia
 ⁶ CSIRO, Space and Astronomy, PO Box 76, Epping NSW 1710 Australia
 ⁷ Astronomy, Astrophysics and Astrophotonics Research Centre, Macquarie University, Sydney, NSW 2109, Australia
 ⁸ ARC Centre of Excellence for All-Sky Astrophysics in 3 Dimensions (ASTRO 3D), Australia
 ⁹ The Oskar Klein Centre, Department of Physics, Stockholm University,
 AlbaNova University Centre, SE 106 91 Stockholm, Sweden

¹⁰ ASTRON, Netherlands Institute for Radio Astronomy, Oude Hoogeveensedijk 4, 7991 PD Dwingeloo, The Netherlands
¹¹ Joint institute for VLBI ERIC, Oude Hoogeveensedijk 4, 7991 PD Dwingeloo, The Netherlands
¹² Centre for Astrophysics and Supercomputing, Swinburne University of Technology, Mail Number H29, PO Box 218, 31122, Hawthorn, VIC, Australia

¹³ARC Centre of Excellence for Gravitational Wave Discovery (OzGrav), Australia

ABSTRACT

The FLIMFLAM survey is collecting spectroscopic data of field galaxies near fast radio burst (FRB) sightlines to constrain key parameters describing the distribution of matter in the Universe. In this work, we leverage the survey data to determine the source of the excess extragalactic dispersion measure (DM), compared to the Macquart relation estimate of four FRBs: FRB20190714A, FRB20200906A, FRB20200430A, and FRB20210117A. By modeling the gas distribution around the foreground galaxy halos and galaxy groups of the sightlines, we estimate $\rm DM_{halos}$, their contribution to the FRB dispersion measures. The FRB20190714A sightline shows a clear excess of foreground halos which contribute roughly $2/3^{rd}$ of the observed excess DM, thus implying a sightline that is baryon-dense. FRB20200906A shows a smaller but non-negligible foreground halo contribution, and further analysis of the IGM is necessary to ascertain the true cosmic contribution to its DM. FRB20200430A and FRB20210117A show negligible foreground contributions, implying a large host galaxy excess and/or progenitor environment excess.

Keywords: galaxies: halos, galaxies: evolution, galaxies: intergalactic medium

1. INTRODUCTION

With the advent of the concordance Lambda-Cold Dark Matter (Λ CDM) cosmological paradigm, there is now a comprehensive model for the large-scale structure of matter in the universe, and its formation under the influence of gravity is one of the key tests that is ac-

Corresponding author: Sunil Simha shassans@ucsc.edu

* Veni fellow

tively being researched. Cosmic microwave background (CMB) experiments (e.g. Bennett et al. 2013; Planck Collaboration et al. 2020) have precisely measured the contents of the universe and simulations have rendered clarity regading the time-evolution of structure beginning from primordial fluctuations (e.g. Springel et al. 2005). In the current paradigm, dark matter forms the cosmic web, the large scale structure that includes voids, filaments, and dense halos and serves as scaffolding for the accretion of baryonic matter. Indeed, hydrodynamical simulations (e.g. Martizzi et al. 2019; Velliscig et al.

2015; Lee et al. 2021) have shown us that the ionized gas populates dark matter halos and also occupies the cosmic web filaments or the intergalactic medium (IGM), albeit in a much more diffuse state.

The low density of the IGM plasma has long challenged baryon census studies at $z \lesssim 0.5$. The Lyman alpha forest and UV absorption studies of metal ion tracers such as OVI and OVII are not sensitive to $\sim 40\%$ of the IGM baryons (i.e. the Missing-Baryon Problem; Fukugita et al. 1998; Shull et al. 2012) which reside is the hot ($\sim 10^6~K$), diffuse phase according to theory (e.g. Cen & Ostriker 2006). With existing facilities, very long-exposure X-ray observations (multimillion seconds) are required to to detect the weak absorption expected from OVII tracers of the hot phase (e.g. Nicastro et al. 2018). Alternatively, stacking the weak kinetic Sunyaev-Zeldovich signal between $\gtrsim 10^6$ galaxy pairs could reveal the gas in filaments (de Graaff et al. 2019).

In the meantime, the serendipitous discovery of the first Fast Radio Burst (FRB) in archival data (Lorimer et al. 2007) has set in motion a series of paradigmchanging discoveries. FRBs are millisecond-duration radio transients whose origins are still widely debated. With improved radio detection techniques, over the last five years multiple FRBs have been localized in the sky with sub-arcsecond accuracy (Tendulkar et al. 2017; Bannister et al. 2019; Law et al. 2020; Bhardwaj et al. 2021) and thus their radial distance could be confidently measured from their host galaxy redshifts (z_{FRB}) . FRBs pulses are dispersed by plasma during propagation and the extent of this effect is directly related to the integrated, line-of-sight free electron density (n_e) . This effect is quantified by the FRB Dispersion Measure (DM_{FRB}) which is defined as:

$$DM_{FRB} = \int \frac{n_e}{1+z} dl \quad . \tag{1}$$

Here, z is the cosmological redshift and dl is the distance element along the line-of-sight. As $\mathrm{DM_{FRB}}$ is an integral quantity, it may be represented as the sum of the electron reservoirs encountered during propagation. i.e.

$$DM_{FRB} = DM_{MW} + DM_{cosmic} + DM_{host}.$$
 (2)

Here, DM_{MW} is from the electrons within the Milky Way interstellar medium (ISM) and halo, DM_{host} is from the counterpart structures in the host galaxy, and DM_{cosmic} is from the plasma in intervening halos and the diffuse IGM in the foreground, i.e. $DM_{cosmic} = DM_{halos} + DM_{IGM}$. Macquart et al. (2020) were the first to estimate DM_{cosmic} for a sample of localized FRBs

and showed that it is correlated with $z_{\rm FRB}$. This was as expected of the current paradigm of cosmological expansion and the fraction of ionized baryons in the universe 1 . This proved directly that the "Missing" Baryons were not just found, but also that DM_{FRB} could viably probe the diffuse plasma in the Universe. The community has largely adopted the moniker of the "Macquart relation" to refer to the average DM_{cosmic}, i.e. $\langle {\rm DM_{cosmic}} \rangle$, versus $z_{\rm FRB}$.

While the mean Macquart relation is well described by cosmology (e.g. Inoue 2004), there is expected to be scatter about DM_{cosmic} at any given redshift due to the inhomgeneity of cosmic structure. For example, some FRB sightlines may intersect the gas rich environments of intra galaxy cluster media while others may primarily intersect cosmic voids. Furthermore, galaxy feedback can influence the variance in gas density by distributing gas further out of gravitational wells (e.g. Prochaska & Zheng 2019). Indeed, as we shall show in the subsequent section, one identifies a number of FRBs where estimates for DM_{cosmic} from nominal assumptions on DM_{host} imply $DM_{cosmic} > \langle DM_{cosmic} \rangle$. However, it is not evident a priori if the excess arises from foreground structure (i.e. intervening halos and IGM overdensities) or from an atypical host and progenitor environment. Our previous work (Simha et al. 2020, 2021) has introduced a methology to estimate the contribution from foreground halos. Here, we apply our analysis to four FRB sightlines with apparently high DM_{cosmic} values. Future application of such analyses on a statistical sample of FRBs can inform us on the distribution of ionized gas within dark matter halos (e.g. McQuinn 2014; Prochaska & Zheng 2019; Lee et al. 2022).

To this end, we leverage the redshifts of galaxies collected as part of the FRB Line-of-Sight Ionization Measurement From Lightcone AAOmega Mapping (FLIM-FLAM) survey (Lee et al. 2022). This redshift survey aims to study the foreground matter distribution along ~ 30 FRB sightlines. The key results expected from the survey include constraints accurate to $\sim 10\%$ on (1) the fraction of baryons in the universe in the diffuse IGM and (2) the fraction of baryons residing in circum-galactic halos that are in the ionized phase. In this redshift survey, spectroscopic redshifts and photometry of foreground galaxies within ~ 1 degree of an FRB sightline are used to generate bespoke models of the line-of-sight ionized matter density tailored to individual lines-of-sight, which can then be compared with the

¹ Estimated by leveraging observational constraints on denser baryon reservoirs in the form of stars, remnants and neutral gas (e.g. Fukugita 2004; Macquart et al. 2020).

DM from the FRB. Key reservoirs of said matter include intervening dark matter halos and the diffuse intergalactic medium (IGM). In this work, with a subset of the spectroscopic data collected, we investigate four excess $\rm DM_{\rm cosmic}$ sightlines: FRB20190714A, FRB20200430A, FRB20200906A and FRB20210117A. These fields were targeted with the wide-field Anglo-Australian Telescope(AAT)/AAOmega and the Keck/LRIS and DEIMOS spectrographs.

This manuscript is outlined as follows: section 2 describes the data collection and reduction. Section 3 describes our intervening-galaxy-halo DM estimation procedure. Section 4 describes the results and section 5 discusses their implications. Throughout this work, unless otherwise specified, we assume a Λ CDM cosmology with Planck 2018 cosmological parameters (Planck Collaboration et al. 2020).

2. DATA

2.1. Sample selection

As described in the introduction, structure in the cosmic web is expected to produce a significant scatter in the Macquart relation due to sightline-to-sightline variation in the column density of intervening gas (Macquart et al. 2020). Figure 1 is an updated plot showing the Macquart relation and data from the sample of CRAFT-localized FRBs published to date (Macquart et al. 2019; Bhandari et al. 2019; Qiu et al. 2019; James et al. 2022a). The DM values shown in the plot correspond to estimates of the cosmic dispersion measures,

$$DM_{cosmic}^{est} = DM_{FRB} - DM_{MW} - \overline{DM_{host}}/(1+z),$$
 (3)

where DM_{MW} is estimated as the sum of the ISM contribution $(DM_{MW,ISM})$ taken from the NE2001 model (Cordes & Lazio 2003), and the halo contribution $(DM_{MW,halo})$ which is assumed to be 40 pc cm⁻³. We do note that there is evidence pointing to highly variable Milky Way halo contribution, DM_{MW,halo}. i.e. $\sigma({\rm DM_{MW,halo}}) \sim 100~{\rm pc\,cm^{-3}}.$ For example, Das et al. (2021) use X-ray absorption lines in quasar spectra from gas within the Milky Way CGM and constrain DM_{MW,halo} along numerous sightlines. Though we did not find a matching absorption sightline from their dataset within 3 degrees of our FRBs we acknowledge the possibility of large DM_{MW,halo}. Studies such as Cook et al. (2023) and Ravi et al. (2023) involving low DM_{FRB} sightlines ($\lesssim 100 \text{ pc cm}^{-3}$) place tighter constraints ($DM_{MW,halo} = 28 - 111 \text{ pc cm}^{-3}$). In this context, we concede our assumption for $\mathrm{DM}_{\mathrm{MW,halo}}$ is probably low but has little impact on our qualitative findings. Furthermore, for Figure 1, we assume a median

host contribution of $\overline{\rm DM_{host}} = 186~{\rm pc\,cm^{-3}}$. A primary goal of this paper is to distinguish between these two scenarios, i.e. the excess arising from the foreground or the FRB host, along individual sightlines.

The blue shading visualizes the expected probability density of $\mathrm{DM_{cosmic}}$ at each redshift, $p(\mathrm{DM_{cosmic}}|z)$, with an assumed feedback parameter F=0.31 (Macquart et al. 2020; McQuinn 2014). The long, low-probability tail in $p(\mathrm{DM_{cosmic}}|z)$ to high $\mathrm{DM_{cosmic}}$ values is due to massive halos of galaxy clusters and groups, which occasionally intersect a sightline. One sees that a sizable fraction of the FRB sample lies above the Macquart relation, and a subset have $\mathrm{DM_{cosmic}^{est}}$ values at or beyond the 80th percentile of the expected distribution at their redshifts. Naively, assuming that our ansatz for $\overline{\mathrm{DM_{host}}}$ is correct, one would expect only 20% (i.e. \sim 4) of the sightlines on average above the 80th percentile for the sample size shown in the figure. However, we find 11.

The FRBs with $\mathrm{DM_{cosmic}^{est}} > \langle \mathrm{DM_{cosmic}} \rangle$ may arise from higher host contributions than the assumed average (i.e. $DM_{host} > \overline{DM_{host}}$) or a larger than average foreground contribution to DM_{cosmic}, or both. Of the 11 FRBs with this apparent excess in DM_{cosmic}, 6 have been targeted in the FLIMFLAM survey and have both shallow, wide-field ($m_r < 20$ mag within 1.1 deg radius around the FRB) AAT/AAOmega spectroscopy, plus deeper, narrow-field spectra ($m_r < 23$ within ~ 5 arcmin radius) using the Keck/LRIS and Keck/DEIMOS instruments. One field, FRB20190608A was previously studied by Simha et al. (2020) using redshift data from SDSS and KCWI integral-field unit observations. In a separate paper, we will use a slightly different methodology to analyze the foreground contribution to the well-studied high-DM source FRB20190520B (Lee et al., in prep). In this work, we present the foreground analysis of the other four fields: FRB20190714A, FRB20200430A, FRB20200906A and FRB20210117A. All of these have $\mathrm{DM}^{\mathrm{est}}_{\mathrm{cosmic}}$ near or beyond the 80th percentile in $p(DM_{cosmic}|z)$ as listed in Table 1.

2.2. Spectroscopic target selection

Field galaxies within a radius of 1.1 degrees of the sightlines were targeted using the fiber-fed AAOmega spectrograph on the 3.9m Anglo-Australian Telescope (AAT) at Siding Spring, Australia. For two fields (FRB20190714A and FRB20210117A), the fiber configurations were designed to target sources with $m_r < 19.4$ mag that were well-resolved in the Pan-STARRS imaging, i.e. distinct from point sources. For fields FRB20200430Aand FRB20200906A, the target criterion is $m_r < 19.2$ mag and $m_r < 19.8$ mag respectively

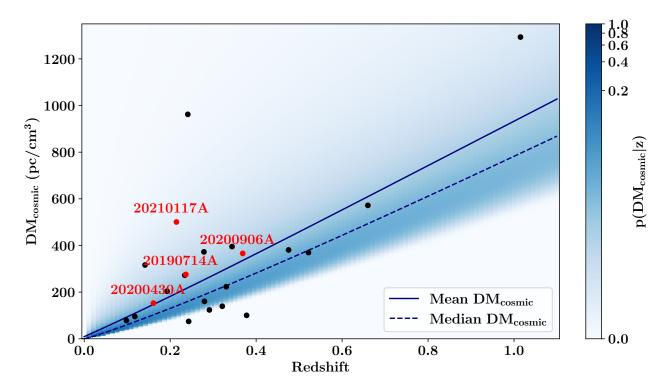


Figure 1. An updated Macquart relation plot including published well-localized FRBs from CRAFT at z < 0.7. The solid line is the mean $\langle \mathrm{DM_{cosmic}} \rangle$ from a universe with the $\Lambda\mathrm{CDM}$ cosmology, a.k.a. the Macquart relation. The blue shading represents $p(\mathrm{DM_{cosmic}}|z)$, the PDF of $\mathrm{DM_{cosmic}}$ at each redshift given the variance in the matter density along a random sightline in the universe from intervening halos and the gas in the cosmic web filaments. Note the median of the distribution (dashed line) lies lower than the mean, implying that most sightlines are expected to have few intervening foreground halos that contribute significantly to $\mathrm{DM_{cosmic}}$. The data points are estimates $\mathrm{DM_{cosmic}^{est}}$ for FRBs from the CRAFT survey. These are the observed $\mathrm{DM_{FRB}}$ corrected for the Milky Way contribution and an assumed host contribution of $\mathrm{\overline{DM_{host}}} = 186~\mathrm{pc~cm^{-3}}$ in the rest frame. The sightlines examined in this work are marked in red, all of which have $\mathrm{DM_{cosmic}} > \langle \mathrm{DM_{cosmic}} \rangle$. Of the other notably high $\mathrm{DM_{cosmic}^{est}}$ sources, FRB20190520B ($z_{\mathrm{FRB}} \sim 0.23$) at $\sim 1000~\mathrm{pc~cm^{-3}}$ will be analyzed in a future work.

Table 1. Our sample

FRB	RA	Dec	Redshift	$\mathrm{DM}_{\mathrm{FRB}}$	$\langle \mathrm{DM_{cosmic}} \rangle$	$\mathrm{DM^{est}_{cosmic}}$	Percentile
	deg	deg		$\rm pccm^{-3}$	$ m pccm^{-3}$	$ m pccm^{-3}$	
FRB20190714A	183.97971	-13.02100	0.2365	504.1	205	275	88
FRB20200430A	229.70642	12.37675	0.1610	380.0	137	152	81
FRB20200906A	53.49617	-14.08318	0.3688	577.8	326	366	82
FRB20210117A	339.97929	-16.15142	0.2145	731.0	185	502	97

Notes: $\langle \mathrm{DM_{cosmic}} \rangle$ is the mean $\mathrm{DM_{cosmic}}$ at the FRB redshift. $\mathrm{DM_{cosmic}^{est}}$ is the estimated $\mathrm{DM_{cosmic}}$ value for the FRB based on $\mathrm{DM_{FRB}}$ and an assumed $\mathrm{\overline{DM_{host}}} = 186~\mathrm{pc\,cm^{-3}}$. Percentile is the percentage of FRBs expected to have $\mathrm{DM_{cosmic}} < \mathrm{DM_{cosmic}^{est}}$ at the FRB redshift.

that were well-resolved in DECam imaging from archival DESI Legacy Imaging Surveys data (Dey et al. 2019). Due to unfavorable weather conditions, we were unable to observe the full roster of fiber configurations generated for FRB20200430A, and so this field has sparser wide-field coverage than intended. We therefore sup-

plement our spectroscopic data on this field from the SDSS database. Each fiber configuration was observed for ~ 1 hr in the 1x1 binning mode with the 570 nm dichroic, which split the light into red and blue components. The red camera used the 385R grating blazed at 720nm while the blue camera used the 580V grat-

ing and the blaze is set to 485nm. The red and blue spectra were reduced, coadded and combined using the 2dFDR version 6.2 based on python 2.7 kindly provided by the OzDES group (Yuan et al. 2015; Childress et al. 2017). We used the MARZ (Hinton et al. 2016) software to determine redshifts, which cross-correlates the input spectra with a set of templates and determines the best redshift. This was followed by a visual inspection to confirm the redshifts, with adjustments as necessary. Figure 2 shows the histogram of redshifts obtained from the AAT for the fields analyzed in this paper. The spectroscopic success rate of the survey, which is defined by the fraction of the number of targets with secure redshift and the total number of the targets that were observed, is around 90%.

In addition, the FRB fields were targeted with the Keck DEIMOS and LRIS spectrographs in the multiobject spectroscopy mode.

We used Pan-STARRS r-band imaging to select $m_r < 23$ mag galaxies (i.e. as before, rejecting point sources) within ~ 5 arcmin of the sightline. To further limit sources to $z \lesssim 0.3$, we rejected sources that satisfy these color criteria based on our analysis of mock galaxy photometry (Lee et al. 2022):

$$g-r > 0$$

 $r-i > 0.7$
 $i > 20.5$ (4)

With LRIS, multi-object slitmask-based spectroscopy of the target galaxies was performed. Our configuration was as follows: 600/7500 grating for the red-side, 600/4000 grism for the blue side and the 560D dichroic. All raw frames were binned 2x2. The LRIS observations were obtained only for the fields of FRB20190714A and FRB20200430A during a previous run and not all objects in the field could be covered due to limited time. The galaxies that were omitted were subsequently targeted with DEIMOS. All LRIS/DEIMOS spectra were reduced with v1.2 of the PypeIt package (Prochaska et al. 2020) package. We set a detection threshold of 3σ above the noise floor for object identification and forced detection for fainter objects using the slitmask information stored in the metadata of the raw frames. Our DEIMOS observations were obtained on a later run with the 600ZD grating and GG455 order blocking filter and 1x1 binning. Each mask configuration was observed for ~ 50 min. Together, 95% of the candidate galaxies within 5 arcmin of the FRB were targeted.

We ignored the serendipitous spectra, i.e. spectra of non-targeted sources captured in our slits, as they generally had no discernible features for redshift assignment. We did not flux-calibrate the spectra as this is not necessary for redshift estimation from line features.

As with the AAT spectra, all reduced spectra from Keck were processed via MARZ (Hinton et al. 2016) to determine redshifts, followed by a visual inspection. As with the AAT data, of the targeted Keck spectra, > 90% had good redshift assignments.

In the case of FRB20190714A, Marnoch (2023, in prep.,) have presented MUSE IFU pointing of 0.67 hours with the Wide Field Mode (WFM) covering the $1' \times 1'$ area around the FRB sightline. Of the 61 galaxies extracted from the stacked white light image (i.e. the image averaged over the spectral dimension), 7 were identified to be foreground sources.

The reduced spectra with their assigned redshifts are made available as a specDB (Prochaska 2017) file ². This is an HDF5 file with the convenience functions from the specDB package for easy retrieval of data.

2.3. Photometric data

To estimate foreground galaxy properties such as stellar mass, we fit the publicly available flux measurements with a spectral energy distribution (SED) model. To this end, we used the *grizy* photometry from the Pan-STARRS (Kaiser et al. 2010) catalog, W1, W2, W3, and W4 from the WISE All-Sky source catalog (Wright et al. 2010) and supplemented with the YJHKs photometry from the Vista Hemisphere Survey (VHS) catalog (Arnaboldi et al. 2007) where available. The details regarding the SED fitting procedure are elucidated in the following section.

3. DM HALO ANALYSIS

In this section, we describe the methodology implemented to estimate the dispersion measure contributed from the halo of a galaxy or group of galaxies, $\mathrm{DM}_{\mathrm{halo}}$. We refer to the summed quantity along a given sightline as $\mathrm{DM}_{\mathrm{halos}}$.

3.1. Individual Halos

Once spectroscopic redshifts were assigned, the available photometry was fit with an SED using CIGALE (Noll et al. 2009). We assumed a delayed-exponential star-formation history with no burst population, a synthetic stellar population prescribed by Bruzual & Charlot (2003), the Chabrier (2003) initial mass function (IMF), dust attenuation models from Calzetti (2001), and dust emission templates from Dale et al. (2014), where the AGN fraction was capped at 20%. This pro-

² Available at this Google Drive link

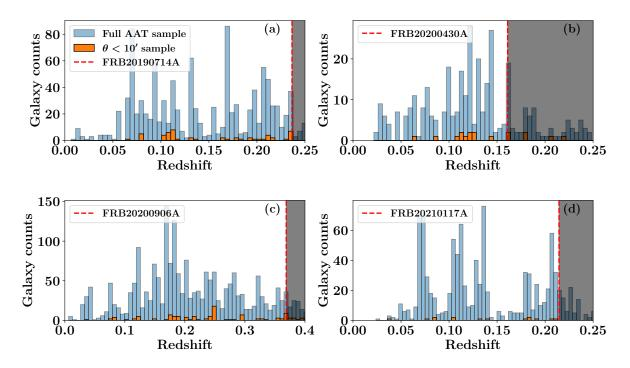


Figure 2. Histogram of galaxy redshifts obtained from the AAOmega spectrograph in the four fields. The full 1.1 degree radius sample is shown in blue and the subset of galaxies within 10 arcmin is shown in orange. The FRB redshift is marked by the dashed red line, and the shaded region represents background galaxies that are not relevant to this study

vided an estimate of the stellar mass, M_* , of the fore-ground galaxy at a given redshift $z_{\rm fg}$.

We then translate M_* to galactic halo mass, $M_{\rm halo}$, using the mean stellar to halo mass relation (SHMR) described by Moster et al. (2013) at that $z_{\rm fg}$. Subsequently, DM_{halo} were estimated using the Prochaska & Zheng (2019) modified NFW halo profile model. We assumed that the total amount of baryons in the halo trace the cosmic mean (Ω_b/Ω_m) . We assumed the halo gas extends to one virial radius (r_{vir}) and that 75% of the baryons are in the hot, ionized phase in the halo. This assumes that 25% of the baryons in the galaxy is in condensed forms (e.g. stars and neutral gas; see Fukugita et al. 1998). While this fraction may vary with halo properties (e.g. Behroozi et al. 2010) or assumptions on galaxy feedback (Sorini et al. 2022; Ayromlou et al. 2022), we emphasize that this is a relatively conservative maximal model for the CGM of galaxies, i.e. one may consider the DM estimates as upper limits. Adopting this CGM model, we then integrate the dispersion measure of the gas at the observed impact parameter R_{\perp} of the galaxy from the sightline determined from its redshift $z_{\rm fg}$ and the angular offset.

The uncertainties in the M_* estimation and the SHMR relation propagate into the $\mathrm{DM}_{\mathrm{halos}}$ estimate. For each

galaxy, we assumed that the $\log M_*$ distribution at a given redshift was Gaussian with the mean and standard deviations obtained from CIGALE. Accounting for the error in the SHMR is more involved as it depends on both M_* and galaxy redshift. The SHMR is described in Equation 2 of Moster et al. (2013) with 8 parameters. We took the best fit parameters and uncertainties from their Table 1 as the mean and standard deviations of the independent normal distributions that these parameters were sampled from. We ignored any co-variance in these fit parameters. From the $\log M_*$ distributions, 1000 samples are drawn and the SHMR parameter space is sampled 1000 times for each $\log M_*$ realization. Thus, for every galaxy, we produce $10^6 \log M_{\rm halo}$ realizations, and subsequently, DM_{halo} estimates. The mean and variance from these individual distributions are used when drawing our conclusions for the sightlines.

3.2. Galaxy group contributions

It is important to account for galaxy groups or clusters, since the overall halo mass is typically much larger than the sum of the putative member masses if estimated individually. This results in DM contributions much greater than that estimated for individual group members. To search for galaxy groups within

the FLIMFLAM spectroscopic catalog, we make use of an anisotropic friends-of-friends (FoF) group finder that has previously been applied to SDSS galaxy survey data (Tago et al. 2008; but see also Tempel et al. 2012,Tempel et al. 2014). This finder assumes a transverse linking length, $d_{\rm LL,\perp}$, which varies as a function of redshift, z, in the following way:

$$d_{\text{LL},\perp}(z) = d_{\text{LL},0}[1 + a\arctan(z/z_*)],$$
 (5)

where $d_{\rm LL,0}$ is the linking length at the initial redshift, whereas a and z_* are parameters governing the redshift evolution. This redshift-dependent linking length allows one, in principle, to account for the declining completeness of the galaxies with increasing redshift in a fluxlimited spectroscopic survey. The line-of-sight linking length, $d_{LL,\parallel}$, is then set as a fixed multiple of $d_{LL,\perp}$; the ratio $d_{\mathrm{LL},\parallel}/d_{\mathrm{LL},\perp}$ is another free parameter for the group finder. To determine the appropriate values for these free parameters, we ran the group finder on the FLIMFLAM catalogs and manually iterated the free parameters of the group finder, while visually inspecting the resulting groups from the FLIMFLAM catalog in both the transverse and line-of-sight dimensions at each iteration. Our criteria was to ensure the selection is not so permissive as to include cosmic web filament structures as part of the identified groups, while simultaneously not being so stringent as to omit the more massive groups at the high-redshift end where the data is typically sparser. We arrived at the following values for the group-finding in this paper: $d_{LL,\perp} = 0.2 h^{-1} \,\mathrm{Mpc}$, $a = 0.75, z_* = 0.1, \text{ and } d_{\text{LL},\parallel}/d_{\text{LL},\perp} = 10.$

To limit ourselves to reasonably robust groups, we select for a minimum richness of $N_{\rm gal} \geq 5$. Furthermore, we apply the same modified NFW profile model; limited still to one virial radius but scaled up to the group mass estimated as our fiducial model. In addition to the coordinates and redshift of each group center, the code also provides a halo mass estimate by applying the virial theorem on the projected group radius and velocity dispersion³.

3.3. Halo Contributions

While our analysis can provide estimates of $\mathrm{DM_{halos}}$ for individual sightlines, it is useful to compare them against a mean cosmic contribution from halos for any random sightline up to z_{FRB} . One may produce a theoretical estimate of this as follows:

Adopting the halo mass function (HMF) (using the implementation of McClintock et al. (2019)) and re-

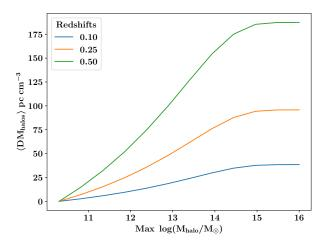


Figure 3. Cumulative estimate of $\langle \mathrm{DM_{halos}} \rangle$ as a function of the maximum halo mass that can contribute to $\mathrm{DM_{halos}}$. $\langle \mathrm{DM_{halos}} \rangle$ is computed assuming the halo mass function corresponding to our adopted cosmology (McClintock et al. 2019), integrated to the given maximum M_{halo} from the same minimum $M_{\mathrm{halo}} = 10^{10.3}\,\mathrm{M}_{\odot}$. The halo gas model has the same modified NFW profile described previously, extending to one virial radius with 75% of the halo baryons in the hot, ionized phase.

stricting ourselves to $M_{\rm halo} < 10^{16}~{\rm M}_{\odot}$, we can estimate the total number of halos of each mass bin expected to intersect within 1 r_{vir} of each sightline. Using our baryon distribution model described in section 3, this can be translated to the average ${\rm DM_{halos}}$ along the sightline, i.e. $\langle {\rm DM_{halos}} \rangle$.

This average represents an upper limit as we are considering halos more massive than those of galaxies. $\langle \mathrm{DM_{halos}} \rangle$ monotonically increases with the halo mass up to which the HMF is integrated over (see Figure 3) but plateaus near $M_{\mathrm{halo}} \approx 10^{15} \mathrm{M_{\odot}}$. This presumably reflects the low average probability of intersecting such massive, but rare, halos. Changing the model parameters that influence $\mathrm{DM_{halo}}$ have similar effect on $\langle \mathrm{DM_{halos}} \rangle$. e.g. increasing the assumed fraction of ionized baryons in the halo scales up both $\mathrm{DM_{halo}}$ and $\langle \mathrm{DM_{halos}} \rangle$ by the same factor.

4. RESULTS

The analysis described above was applied to each galaxy in each field, resulting in probability distributions for the $\rm DM_{halos}$ contribution of individual galaxies and groups. The $\rm DM_{halos}$ value is then the straight sum along each sightline. Our findings from the analysis for each sightline described above are presented in this section.

³ The group catalogs generated for our fields are available at this Google Drive link.

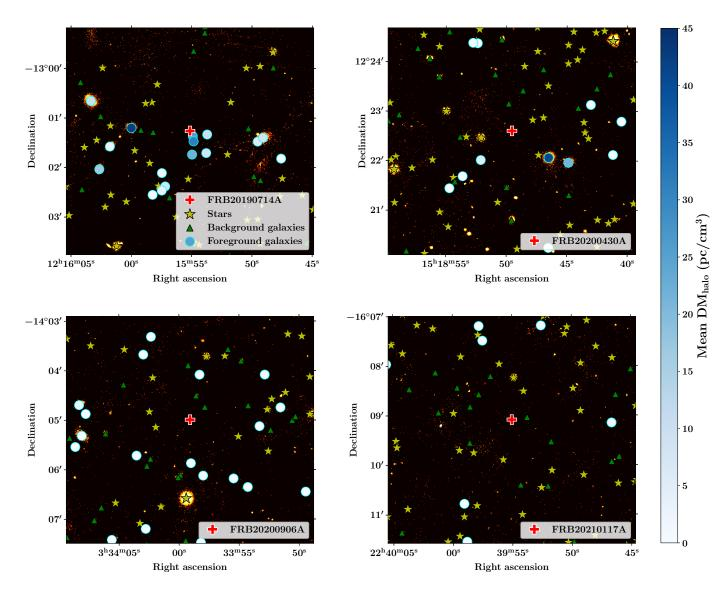


Figure 4. Zoomed-in $(5' \times 5')$ illustration of the fields and results for the four FRB sightlines: (a) FRB20190714A, (b) FRB20200430A, (c) FRB20200906A, and (d) FRB20210117A. The background shows Pan-STARRS r-band images. In each image, the red crosses mark the location of the FRB, the green triangles mark the background galaxies and the yellow stars mark the point sources that were ignored from spectroscopic targeting. The blue circles mark the foreground galaxies, with the color scaled according to the estimated DM_{halo} value.

Figure 4 is a visual summary of the individual fields. It highlights stars, background objects and foreground objects $\lesssim 3$ arcmin of the FRBs on the r-band image of the field from Pan-STARRS. The foreground objects are colored by the average DM_{halo} contribution estimated for each of them.

4.1. FRB20190714A

Examining Figure 4, one notes multiple galaxies in the foreground field of FRB20190714A including several within $\approx 30''$. These galaxies lie primarily at two

redshifts: z=0.10 and 0.21 and have estimated halo masses that yield significant DM_{halo} contributions. The galaxy with the smallest impact parameter (J121554.90-130121.95) was found in the VLT/MUSE datacube and has a redshift of 0.08 yielding a projected perpendicular distance of $R_{\perp}=11\,\mathrm{kpc}$ (Marnoch 2023, in prep.). Even though its mass estimate indicates it is a dwarf galaxy ($M_*=10^{8.5}~\mathrm{M}_{\odot}$), its close proximity to the sightline leads to a substantial DM_{halo} contribution of 25 pc cm⁻³.

Excess FRB DM

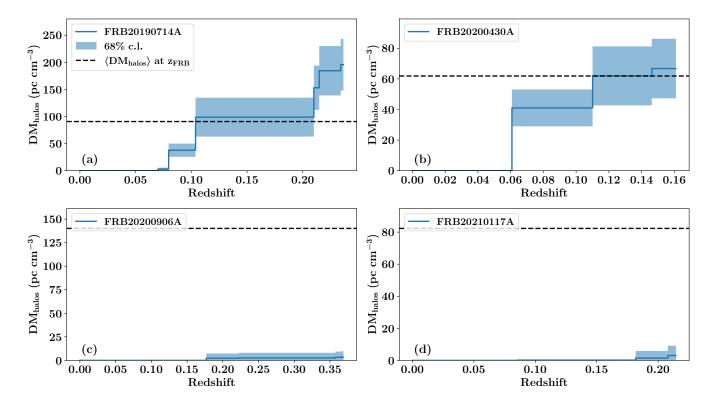


Figure 5. Empirical evaluation of $\mathrm{DM_{halos}}$ for the FRB sightlines as a function of redshift. The blue curve presents the cumulative estimation of $\mathrm{DM_{halos}}$ from z=0, which increases monotonically as foreground halos are encountered along the sightline. The blue shading represents 68% confidence limits on the $\mathrm{DM_{halos}}$ estimate, which is the running quadrature sum of the individual 1-sigma limits of the DM distributions for the individual galaxies. The black dashed lines represent estimates for $\langle \mathrm{DM_{halos}} \rangle$ assuming the our adopted halo mass function (up to $M_{\mathrm{halo}}=10^{16}~\mathrm{M_{\odot}}$) and the adopted halo gas distribution model used to calculate $\mathrm{DM_{halos}}$. While the FRB20190714A sightline clearly exceeds the average expectation, both FRB20210117A and FRB20200906A are barely in excess of $\mathrm{DM_{halos}}=0~\mathrm{pc~cm^{-3}}$. FRB20200430A exhibits a $\mathrm{DM_{halos}}$ value consistent with $\langle \mathrm{DM_{halos}} \rangle$.

The wide-field data from Keck/DEIMOS and LRIS show 110 foreground galaxies, and of these 17 show non-zero $\mathrm{DM_{halo}}$ contributions. Table 2 lists the foreground galaxies and their mean $\mathrm{DM_{halo}}$ contributions 4 .

We do not find any group contribution when applying our fiducial halo gas model, which truncates at the virial radius, to the groups identified in this field. If, however, one extended the model to two virial radii we estimate one of the groups would give a $50\,\mathrm{pc\,cm^{-3}}$ contribution. This group is centered at RA/Dec of (184.1382405, -13.0107427) and z=0.111. The FRB sightline is at a transverse distance of 1.16 Mpc. With 20 member galaxies and a halo mass of $10^{13.9}\mathrm{M}_{\odot}$, this group may potentially contribute to $\mathrm{DM}_{\mathrm{cosmic}}$. We do not include this contribution in our $\mathrm{DM}_{\mathrm{halos}}$ estimate but discuss the implications of doing so in Section 5.

Figure 5a presents the cumulative sum of $\rm DM_{halos}$ with redshift and shows a total value of $200\pm45\,\rm pc\,cm^{-3}$. This exceeds by over $100\,\rm pc\,cm^{-3}$ the average estimated $\langle \rm DM_{halos} \rangle$ for the FRB redshift using the methodology described in Section 3.3. For this FRB, we infer that its $\rm DM_{cosmic}^{est}$ exceeds $\langle \rm DM_{cosmic} \rangle$ owing to an excess of foreground structure. We return to this conclusion in the following section.

4.2. FRB20200430A

While FRB20200430A has the least significant excess value of $\rm DM^{\rm est}_{\rm cosmic}$ in our sample, we estimate that the foreground galaxies in the field of FRB20200430A contribute significantly to $\rm DM_{halos}$, similar to FRB20190714A. Specifically, we estimate $\rm DM_{halos} = 65 \pm 20\,pc\,cm^{-3}$ which is comparable to $\rm \langle DM_{halos} \rangle$ at $z_{\rm FRB} = 0.161$ (Fig. 5b).

We do not find any group contribution to DM_{halos} for this sightline; the closest group lies at 4.6 Mpc transverse distance with a mass of only $10^{13} \, M_{\odot}$. At over ~ 10

 $^{^4}$ The full galaxy catalogs with their halo masses and $\rm DM_{halo}$ estimates for our fields are available at this Google Drive link.

FRB	RA	Dec	$z_{ m fg}$	R_{\perp}	$\log({ m M_*/M_{\odot}})$	$\log({ m M_{halo}/M_{\odot}})$	$\mathrm{DM}_{\mathrm{halo}}$	$\sigma({ m DM_{halo}})$
	deg	deg		kpc			$\rm pccm^{-3}$	$ m pccm^{-3}$
FRB20190714A	184.01105	-13.03391	0.1044	236	10.6	12.2	16.6	16.3
FRB20190714A	183.97902	-13.02895	0.2119	102	10.1	11.7	21.9	10.4
FRB20190714A	183.97876	-13.02276	0.0802	11	8.2	10.7	25.1	4.2
FRB20190714A	183.97849	-13.02450	0.2141	47	9.6	11.4	31.4	20.4
FRB20190714A	183.99997	-13.02000	0.1042	140	10.8	12.4	42.7	29.5
FRB20200430A	229.71715	12.36691	0.1448	135	9.7	11.4	4.8	2.9
FRB20200430A	229.68695	12.36605	0.1109	163	10.5	11.9	21.0	15.0
FRB20200430A	229.69376	12.36773	0.0619	67	10.3	11.8	41.0	12.1
FRB20200906A	53.53467	-14.07823	0.1761	417	11.0	13.1	2.2	5.1
FRB20210117A	339.96901	-16.11978	0.1827	378	10.5	12.0	1.4	4.4
FRB20210117A	339.94438	-16.15251	0.2085	424	10.9	12.8	1.6	4.2

Table 2. Foreground galaxies contributing to DM_{halos} .

virial radii from the sightline, this group has no plausible influence on the observed DM_{halos} .

4.3. FRB20200906A

Although this field exhibits a large number of fore-ground galaxies within 10′ of the FRB including nearly 20 within 5′ of the sightline, we estimate their contributions $\mathrm{DM_{cosmic}}$ to be nearly negligible. Many of these galaxies also have high, estimated halo masses but their individual contributions are generally $\mathrm{DM_{halo}} \lesssim 1~\mathrm{pc~cm^{-3}}$ (Table 2). This results from the the large physical impact parameters; only one has $R_{\perp} < 200~\mathrm{kpc}$ from the sightline.

We estimate no group contribution to DM_{halos} for this field, with the closest group being 860 kpc away with a mass of $10^{11.7} \rm M_{\odot}$ (z=0.04). This comparatively low-mass halo was detected as a group only by virtue of its low redshift (and hence small distance modulus).

$4.4. \;\; FRB20210117A$

From our sample of four FRBs with $\rm DM^{\rm est}_{\rm cosmic} > \langle \rm DM_{\rm cosmic} \rangle$, FRB20210117A is the most extreme outlier with more than $380\,{\rm pc\,cm^{-3}}$ in excess of the average value at the $z_{\rm FRB}=0.2145$. Remarkably, as is evident from Figure 4b, we do not find any foreground halos in close proximity to the sightline. As such, the total $\rm DM_{halos}$ estimate is very small (Figure 5b). The galaxy with the largest $\rm DM_{halo}$ estimate (1.6 pc cm⁻³) is over 400 kpc away and has a halo mass of $10^{12.8}{\rm M}_{\odot}$. Given the uncertainties in halo masses, $\rm DM_{halos}$ is even consistent with 0, i.e. no intersections within one virial radius of any foreground halo.

Not surprisingly, we also find no contribution from the galaxy groups identified in this field. The closest group lies at a distance of $2\,\mathrm{Mpc}$.

5. DISCUSSION

In the previous section we presented our analysis of the foreground matter distribution along four sightlines, with focus on $\mathrm{DM_{halos}}$. We now discuss the implications of these results. The primary motivation of this paper was to explore the origin of apparent excess in $\mathrm{DM_{cosmic}}$ along FRB sightlines. To place our results in this context, we construct an empirical model $\mathrm{DM_{cosmic}^{model}}$ for the four sightlines based on our findings. Specifically, define

$$DM_{cosmic}^{model} = DM_{halos} + \langle DM_{IGM} \rangle$$
 (6)

where $\langle DM_{IGM} \rangle$ is given by

$$\langle \mathrm{DM}_{\mathrm{IGM}} \rangle = \langle \mathrm{DM}_{\mathrm{cosmic}} \rangle - \langle \mathrm{DM}_{\mathrm{halos}} \rangle$$
 (7)

with $\langle \mathrm{DM_{halos}} \rangle$ calculated as described in Section 3.3 and all quantities are evaluated at z_{FRB} . In future analyses the FLIMFLAM survey will estimate $\mathrm{DM_{IGM}}$ for individual fields with the cosmic web reconstruction algorithm ARGO (Ata et al. 2015), which is a Bayesian estimator for the matter density field given the foreground galaxy halo masses and 3D locations (i.e. their sky position and redshifts).

Our DM_{cosmic}^{model} estimate assumes the uncertainty in DM_{halos} (Table 3) and a 20% statistical uncertainty in $\langle DM_{IGM} \rangle$ based on numerical simulations (e.g. Lee et al. 2022) We also emphasize that the assumed CGM model used to estimate DM_{halos} impacts $\langle DM_{halos} \rangle$ and therefore $\langle DM_{IGM} \rangle$ through Equation 7. This sensitivity to the CGM model (here a systematic error) lies central to correlating DM_{FRB} against galactic halos and large-scale structure to constrain properties of halo gas and the baryonic content of the IGM (Lee et al. 2022; Rafiei-Ravandi et al. 2021). In the current analysis, however,

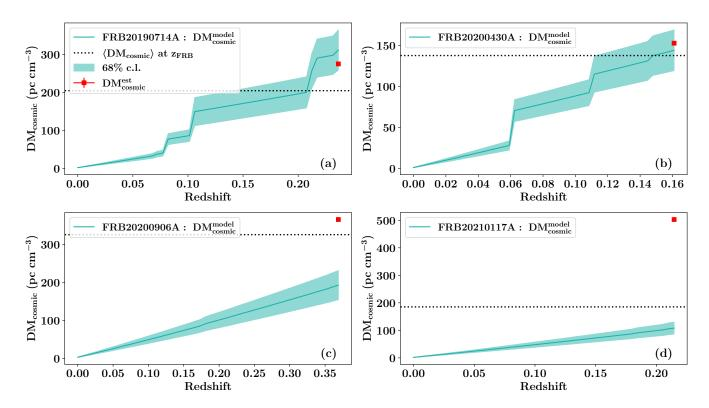


Figure 6. Estimates of DM_{cosmic} for the FRB sightlines as a function of redshift. The solid, teal curve is DM_{cosmic}^{model} , a sum of DM_{halos} , i.e. the solid, blue curve from Figure 5 and an estimate of the average IGM contribution to DM_{cosmic} (see text for details). The dotted line shows $\langle DM_{cosmic} \rangle$ at z_{FRB} in each subplot. The shading around the solid curve represents a 68% confidence limit which includes an assumed 20% uncertainty for $\langle DM_{IGM} \rangle$ in quadrature with the uncertainties from Figure 5. The red point is an estimate of DM_{cosmic} for each FRB taken from Figure 1, i.e. by subtracting the assumed host and Milky Way contributions.

the CGM model has less impact for decreases in DM_{halos} will be compensated by an increase in $\langle DM_{IGM} \rangle$.

Figure 6 presents cumulative estimates for DM^{model}_{cosmic} with redshift for each field. These are compared with $\langle DM_{cosmic} \rangle$ at z_{FRB} and our values for DM_{cosmic}^{est} using Equation 3. As one may have anticipated, $\mathrm{DM_{cosmic}^{model}}$ for the two fields with large $\mathrm{DM_{halos}}$ values (FRB20190714A, FRB20200430A) are consistent with DM_{cosmic} (see also Table 3). For these two FRBs, we have empirical confirmation of the theoretical paradigm for DM_{cosmic}, i.e. that its intrinsic scatter tracks the incidence of foreground structure. These results lend further confidence for future analyses leveraging DM_{FRB} to resolve the cosmic web. Compared to the previously studied sightlines of FRB20190608A (Simha et al. 2020) and FRB20180924B (Simha et al. 2021), FRB20190714A is the first that shows a significantly large contribution from foreground halos. As mentioned previously, such sightlines are expected to be rare (e.g. McQuinn 2014).

On the other hand, the DM $_{\rm cosmic}^{\rm model}$ estimates for FRB20200906A and FRB20210117A do not even meet the average $\langle {\rm DM}_{\rm cosmic} \rangle$ for these sources, much less the

apparent excess implied by $\rm DM_{cosmic}^{est}$. The shortfalls are $\approx 200\,\rm pc\,cm^{-3}$ and $\approx 425\,\rm pc\,cm^{-3}$ respectively. Even accounting for uncertainty in our $\rm DM_{halos}$ and $\rm DM_{IGM}$ estimates, one cannot account for these differences within the $\sim 1\sigma$ uncertainties. This suggests the observed excess is due to a higher than average $\rm DM_{host}$ component; we estimate the rest-frame $\rm DM_{host}$ values to be $\approx 422\,\rm pc\,cm^{-3}$ and $\approx 665\,\rm pc\,cm^{-3}$ respectively. These sightlines are remarkably similar to the that reported by Niu et al. (2022) for FRB20190520B, implying a relatively low $\rm DM_{cosmic}$ compared to $\rm DM_{host}$ for these sightlines. Future detection of such sightlines might be key to unravel the likely progenitor scenarios and in investigating how $\rm DM_{host}$ depends on host galaxy properties.

We may further assess the likelihood of this conclusion as follows. Adopting a lognormal PDF for $\rm DM_{host}$ with the parameters estimated by James et al. (2022b), the fraction of FRBs with $\rm DM_{host}$ values in excess of these estimates are 18% and 9% respectively. The large $\rm DM_{host}$ values can be attributed to a combination of the local progenitor environment and the host ISM.

One may search for signatures of a high DM_{host} value from detailed studies of the host galaxies. FRB20210117A arises in a low-mass (dwarf) galaxy with a low star-formation rate (Bhandari et al. 2023; Gordon et al. 2023). It is offset from the galaxy center by $\approx 3\,\mathrm{kpc}$ which exceeds the half-light radius. In these regards, there is nothing apparent in the host properties nor its inferred halo that would suggest such a large DM_{host} value. Bhandari et al. (2023, in prep.) propose a possible scenario involving the FRB progenitor being embedded in the outflows of a hyper-accreting black hole and note that long-term, short-cadence observations of the FRB polarization may constrain such a model should the FRB repeat.

FRB20200906A on the other hand arises from a high-mass, high-star-formation-rate galaxy and is coincident with the disk of the host (see Figure 1 of Gordon et al. 2023). This implies a fraction of the DM_{host} arises from the host ISM. For example, Chittidi et al. (2021) estimated for FRB20190608B $\sim 90 \text{ pc cm}^{-3}$ for the host ISM contribution from the local H-alpha line emission measure. While Gordon et al. (2023) report slightly lower star-formation rate for the host of FRB20200906A than FRB20190608B, one can visually discern a higher disk inclination for the former and speculate a comparable if not higher DM_{host} for the ISM component. A dedicated optical follow-up study of the host with an integral-field unit, especially if one can resolve \lesssim 1kpc around the FRB, can help place upper limits on the ISM contribution. For all the four FRB host galaxies, if we applied our galaxy halo gas model and computed DM_{halo} as analyzed above, we estimate a contribution of $\lesssim 35 \text{ pc cm}^{-3}$ each.

As mentioned previously, a full IGM reconstruction analysis is necessary for a complete understanding of the foreground matter density, e.g. as done for FRB20190608B (Simha et al. 2020). While we have established two of our fields have $DM_{\rm cosmic}^{\rm model} \sim DM_{\rm cosmic}^{\rm est}$ it is possible that the IGM reconstruction may reveal $DM_{\rm IGM} > \langle DM_{\rm IGM} \rangle$ and therefore lay tighter constraints on $DM_{\rm host}$. With ~ 30 sightlines, the FLIM-FLAM survey will perform such analysis and render, as a useful by-product, a posterior distribution for $DM_{\rm host}$. This distribution can serve as a prior to future FRB-based IGM tomography work as well as to constrain FRB progenitor channels.

6. CONCLUSION

To summarize, we analyzed the galaxies in the foreground of four localized FRBs, whose estimated cosmic dispersion measure $\mathrm{DM}^{\mathrm{est}}_{\mathrm{cosmic}}$ significantly exceeds the

average at z_{FRB} . Implementing the methodology detailed in Section 3, we estimated the DM contribution of foreground galactic and group halos, DM_{halos}, as summarized in Table 3. For two fields, we found a high incidence of halos at close impact parameters to the sightline, such that the DM_{halos} estimate matches or exceeds the average cosmic expectation value, $\langle DM_{halos} \rangle$. For the other two fields, the $\mathrm{DM}_{\mathrm{halos}}$ estimate is less than $5 \,\mathrm{pc}\,\mathrm{cm}^{-3}$ owing to the absence of foreground halos near the sightline. Our results reinforce the paradigm that FRBs can effectively probe foreground matter overdensities. That being said, one must exercise caution in accounting for plasma in the host galaxy and immediate FRB progenitor environment when studying matter distribution along the sightline. Combined with Simha et al. (2020) we conclude FRBs with apparent high DM_{cosmic} arise from both higher than average foreground structure and inferred higher host contributions, with nearly equal probability.

Thus the FLIMFLAM survey is ramping up efforts towards data collection and analysis. Future results are expected to lay robust constraints on the parameters describing foreground matter distribution as well as constrain $\mathrm{DM}_{\mathrm{host}}$ statistically.

ACKNOWLEDGEMENTS

We thank Elmo Tempel for kindly providing his groupfinding software, and Chris Lidman for assistance with the OzDES data reduction pipeline for AAOmega. Authors S.S., J.X.P., and N.T., as members of the Fast and Fortunate for FRB Follow-up team, acknowledge support from NSF grants AST-1911140, AST-1910471 and AST-2206490. N.T. and L.B. acknowledge support by FONDECYT grant 11191217. We acknowledge generous financial support from Kavli IPMU that made FLIMFLAM possible. Kavli IPMU is supported by World Premier International Research Center Initiative (WPI), MEXT, Japan. Based on data acquired at the Anglo-Australian Telescope, under programs A/2020B/04, A/2021A/13, and O/2021A/3001. We acknowledge the traditional custodians of the land on which the AAT stands, the Gamilaraay people, and pay our respects to elders past and present.

Software: MARZ (Hinton et al. 2016), HMFEmulator (McClintock et al. 2019), specDB (Prochaska 2017), CIGALE (Noll et al. 2009), Astropy (Price-Whelan et al. 2018), Numpy (Oliphant 2006), Scipy (Virtanen et al. 2020), Matplotlib (Hunter 2007).

The Python scripts used to perform our analysis are available in our FRB GitHub repository (https://github.com/FRBs/FRB).

FRB	Redshift	$\langle { m DM_{halos}} \rangle$	$\mathrm{DM}_{\mathrm{halos}}$	$\sigma({ m DM_{halos}})$	$\mathrm{DM_{cosmic}^{est}}$	$\mathrm{DM_{cosmic}^{model}}$	$\sigma(\mathrm{DM_{cosmic}^{model}})$
		$ m pccm^{-3}$	$ m pccm^{-3}$	$ m pccm^{-3}$	$ m pccm^{-3}$	$ m pccm^{-3}$	$ m pccm^{-3}$
FRB20190714A	0.2365	92	195	47	275	312	53
FRB20200430A	0.1610	63	66	19	152	144	24
FRB20200906A	0.3688	142	3	4	366	193	38
FRB20210117A	0.2145	83	3	4	502	108	21

Table 3. Summary Table

REFERENCES

- Arnaboldi, M., Neeser, M. J., Parker, L. C., et al. 2007, The Messenger, 127, 28
- Ata, M., Kitaura, F.-S., & Müller, V. 2015, MNRAS, 446, 4250, doi: 10.1093/mnras/stu2347
- Ayromlou, M., Nelson, D., & Pillepich, A. 2022, arXiv e-prints, arXiv:2211.07659, doi: 10.48550/arXiv.2211.07659
- Bannister, K. W., Deller, A. T., Phillips, C., et al. 2019, Science, 365, 565, doi: 10.1126/science.aaw5903
- Behroozi, P. S., Conroy, C., & Wechsler, R. H. 2010, ApJ, 717, 379, doi: 10.1088/0004-637X/717/1/379
- Bennett, C. L., Larson, D., Weiland, J. L., et al. 2013, ApJS, 208, 20, doi: 10.1088/0067-0049/208/2/20
- Bhandari, S., Bannister, K. W., James, C. W., et al. 2019, MNRAS, 486, 70, doi: 10.1093/mnras/stz804
- Bhandari, S., Gordon, A., Scott, D., et al. 2023, apj, submitted
- Bhardwaj, M., Kirichenko, A. Y., Michilli, D., et al. 2021, ApJL, 919, L24, doi: 10.3847/2041-8213/ac223b
- Bruzual, G., & Charlot, S. 2003, MNRAS, 344, 1000, doi: 10.1046/j.1365-8711.2003.06897.x
- Calzetti, D. 2001, PASP, 113, 1449, doi: 10.1086/324269
 Cen, R., & Ostriker, J. P. 2006, ApJ, 650, 560, doi: 10.1086/506505
- Chabrier, G. 2003, PASP, 115, 763, doi: 10.1086/376392
- Childress, M. J., Lidman, C., Davis, T. M., et al. 2017, Monthly Notices of the Royal Astronomical Society, 472, 273, doi: 10.1093/mnras/stx1872
- Chittidi, J. S., Simha, S., Mannings, A., et al. 2021, ApJ, 922, 173, doi: 10.3847/1538-4357/ac2818
- Cook, A. M., Bhardwaj, M., Gaensler, B. M., et al. 2023, ApJ, in press
- Cordes, J. M., & Lazio, T. J. W. 2003, ArXiv Astrophysics e-prints
- Dale, D. A., Helou, G., Magdis, G. E., et al. 2014, ApJ, 784, 83, doi: 10.1088/0004-637X/784/1/83
- Das, S., Mathur, S., Gupta, A., Nicastro, F., & Krongold, Y. 2021, MNRAS, 500, 655, doi: 10.1093/mnras/staa3299

- de Graaff, A., Cai, Y.-C., Heymans, C., & Peacock, J. A. 2019, A&A, 624, A48, doi: 10.1051/0004-6361/201935159
- Dey, A., Schlegel, D. J., Lang, D., et al. 2019, AJ, 157, 168, doi: 10.3847/1538-3881/ab089d
- Fukugita, M. 2004, Symposium International Astronomical Union, 220, 227–232, doi: 10.1017/S0074180900183287
- Fukugita, M., Hogan, C. J., & Peebles, P. J. E. 1998, ApJ, 503, 518, doi: 10.1086/306025
- Gordon, A. C., Fong, W.-f., Kilpatrick, C. D., et al. 2023, arXiv e-prints, arXiv:2302.05465. https://arxiv.org/abs/2302.05465
- Hinton, S. R., Davis, T. M., Lidman, C., Glazebrook, K., & Lewis, G. F. 2016, Astronomy and Computing, 15, 61, doi: 10.1016/j.ascom.2016.03.001
- Hunter, J. D. 2007, Computing in Science & Engineering, 9, 90, doi: 10.1109/MCSE.2007.55
- Inoue, S. 2004, MNRAS, 348, 999, doi: 10.1111/j.1365-2966.2004.07359.x
- James, C. W., Prochaska, J. X., Macquart, J. P., et al. 2022a, MNRAS, 509, 4775, doi: 10.1093/mnras/stab3051
- James, C. W., Ghosh, E. M., Prochaska, J. X., et al. 2022b, arXiv e-prints, arXiv:2208.00819. https://arxiv.org/abs/2208.00819
- Kaiser, N., Burgett, W., Chambers, K., et al. 2010, in Society of Photo-Optical Instrumentation Engineers (SPIE) Conference Series, Vol. 7733, Ground-based and Airborne Telescopes III, ed. L. M. Stepp, R. Gilmozzi, & H. J. Hall, 77330E, doi: 10.1117/12.859188
- Law, C. J., Butler, B. J., Prochaska, J. X., et al. 2020, ApJ, 899, 161, doi: 10.3847/1538-4357/aba4ac
- Lee, J., Shin, J., Snaith, O. N., et al. 2021, ApJ, 908, 11, doi: 10.3847/1538-4357/abd08b
- Lee, K.-G., Ata, M., Khrykin, I. S., et al. 2022, ApJ, 928, 9, doi: 10.3847/1538-4357/ac4f62
- Lorimer, D. R., Bailes, M., McLaughlin, M. A., Narkevic, D. J., & Crawford, F. 2007, Science, 318, 777, doi: 10.1126/science.1147532

Macquart, J. P., Shannon, R. M., Bannister, K. W., et al. 2019, ApJL, 872, L19, doi: 10.3847/2041-8213/ab03d6

- Macquart, J. P., Prochaska, J. X., McQuinn, M., et al. 2020, Nature, 581, 391, doi: 10.1038/s41586-020-2300-2
- Marnoch, L. 2023, ApJ, in prep
- Martizzi, D., Vogelsberger, M., Artale, M. C., et al. 2019, MNRAS, 486, 3766, doi: 10.1093/mnras/stz1106
- McClintock, T., Rozo, E., Becker, M. R., et al. 2019, ApJ, 872, 53, doi: 10.3847/1538-4357/aaf568
- McQuinn, M. 2014, ApJL, 780, L33, doi: 10.1088/2041-8205/780/2/L33
- Moster, B. P., Naab, T., & White, S. D. M. 2013, MNRAS, 428, 3121, doi: 10.1093/mnras/sts261
- Nicastro, F., Kaastra, J., Krongold, Y., et al. 2018, Nature, 558, 406, doi: 10.1038/s41586-018-0204-1
- Niu, C. H., Aggarwal, K., Li, D., et al. 2022, Nature, 606, 873, doi: 10.1038/s41586-022-04755-5
- Noll, S., Burgarella, D., Giovannoli, E., et al. 2009, A&A, 507, 1793, doi: 10.1051/0004-6361/200912497
- Oliphant, T. E. 2006, A guide to NumPy, Vol. 1 (Trelgol Publishing USA)
- Planck Collaboration, Aghanim, N., Akrami, Y., et al. 2020, A&A, 641, A6, doi: 10.1051/0004-6361/201833910
- Price-Whelan, A. M., Sipőcz, B. M., Günther, H. M., et al. 2018, AJ, 156, 123, doi: 10.3847/1538-3881/aabc4f
- Prochaska, J., Hennawi, J., Westfall, K., et al. 2020, The Journal of Open Source Software, 5, 2308, doi: 10.21105/joss.02308
- Prochaska, J. X. 2017, Astronomy and Computing, 19, 27, doi: 10.1016/j.ascom.2017.03.003
- Prochaska, J. X., & Zheng, Y. 2019, MNRAS, 485, 648, doi: 10.1093/mnras/stz261

- Qiu, H., Bannister, K. W., Shannon, R. M., et al. 2019, MNRAS, 486, 166, doi: 10.1093/mnras/stz748
- Rafiei-Ravandi, M., Smith, K. M., Li, D., et al. 2021, ApJ, 922, 42, doi: 10.3847/1538-4357/ac1dab
- Ravi, V., Catha, M., Chen, G., et al. 2023, aas, in press
 Shull, J. M., Smith, B. D., & Danforth, C. W. 2012, ApJ, 759, 23, doi: 10.1088/0004-637X/759/1/23
- Simha, S., Burchett, J. N., Prochaska, J. X., et al. 2020, ApJ, 901, 134, doi: 10.3847/1538-4357/abafc3
- Simha, S., Tejos, N., Prochaska, J. X., et al. 2021, ApJ, 921, 134, doi: 10.3847/1538-4357/ac2000
- Sorini, D., Davé, R., Cui, W., & Appleby, S. 2022, MNRAS, 516, 883, doi: 10.1093/mnras/stac2214
- Springel, V., White, S. D. M., Jenkins, A., et al. 2005, Nature, 435, 629, doi: 10.1038/nature03597
- Tago, E., Einasto, J., Saar, E., et al. 2008, A&A, 479, 927, doi: 10.1051/0004-6361:20078036
- Tempel, E., Kipper, R., Saar, E., et al. 2014, A&A, 572, A8, doi: 10.1051/0004-6361/201424418
- Tempel, E., Tago, E., & Liivamägi, L. J. 2012, A&A, 540, A106, doi: 10.1051/0004-6361/201118687
- Tendulkar, S. P., Bassa, C. G., Cordes, J. M., et al. 2017, ApJL, 834, L7, doi: 10.3847/2041-8213/834/2/L7
- Velliscig, M., Cacciato, M., Schaye, J., et al. 2015, MNRAS, 453, 721, doi: 10.1093/mnras/stv1690
- Virtanen, P., Gommers, R., Oliphant, T. E., et al. 2020, Nature Methods, 17, 261,
 - doi: https://doi.org/10.1038/s41592-019-0686-2
- Wright, E. L., Eisenhardt, P. R. M., Mainzer, A. K., et al. 2010, AJ, 140, 1868, doi: 10.1088/0004-6256/140/6/1868
- Yuan, F., Lidman, C., Davis, T. M., et al. 2015, Monthly Notices of the Royal Astronomical Society, 452, 3047, doi: 10.1093/mnras/stv1507